Gradient-based sizing optimization of power-beaming-enabled aircraft

Nicholas C. Orndorff*, Bingran Wang†, Marius L. Ruh‡, Andrew H. Fletcher§, and John T. Hwang¶
University of California San Diego, La Jolla, CA, 92092

Power beaming is a potentially disruptive technology for aircraft that would lead to unprecedented increases in some aspects of mission performance. Existing aircraft design methods often rely on empirical data and energy-based formulas for size and performance estimations. These methods are not applicable to power-beaming-enabled aircraft, which have reduced needs for onboard energy storage. In this paper, we investigate the dominant variables that have the strongest influence on the size and design of a laser-powered, unmanned, high-altitude aircraft. This is accomplished by constructing several physics-based models within a large-scale design optimization framework. Using this framework, we perform a baseline optimization that minimizes total mass, demonstrating that our method can produce a feasible and optimal airplane design. By varying several parameters within the optimization problem we also determine the sensitivity of the airplane design to altitude, payload, endurance, and distance from the laser source. Among other things, we find that total mass increases exponentially with onboard battery power, and that total mass increases very little with distance until 600 km after which the mass begins to increase exponentially.

I. Nomenclature

u, v, w	=	linear velocity in the body-fixed frame (m/s)
p, q, r	=	angular velocity in the body-fixed frame (m/s)
x, y, z	=	position in the Earth-fixed frame (m)
ϕ, θ, ψ	=	Euler angles (rad)
F_x, F_y, F_z	=	net forces in the body-fixed frame (N)
L, M, N	=	moments in the body-fixed frame (N·m)
$m, I_{(\cdot)}$	=	mass (kg) and mass-moment of inertia (kg·m^2)
$\mathcal{R}$	=	trim residual (m^2/s^4)
R_o	=	optical power residual (W)
C_P, C_Q, C_T	=	thrust, torque, and power coefficients
d_r	=	rotor diameter (m)
b	=	wing span (m)
d_a	=	aperture diameter (m)
$t_\text{cap}, t_\text{web}$	=	box-beam web and cap thickness (m)
h	=	convective heat transfer coefficient (W/m^2·K)
Nu, Pr, Re	=	Nusselt, Prandtl, and Reynolds numbers
C_L, C_D	=	lift and drag coefficients
T_s, T_∞	=	surface temperature and free-stream flow temperature (°K)
A	=	heat transfer surface area (m^2)
$\dot{Q}$	=	heat transfer rate (W)
λ	=	wavelength (m)

*Ph.D Student, Department of Mechanical and Aerospace Engineering, AIAA Student Member
†Ph.D Candidate, Department of Mechanical and Aerospace Engineering, AIAA Student Member
‡Ph.D Student, Department of Mechanical and Aerospace Engineering, AIAA Student Member
§Ph.D Student, Department of Mechanical and Aerospace Engineering, AIAA Student Member
¶Assistant Professor, Department of Mechanical and Aerospace Engineering, AIAA Member.

II. Introduction

Aircraft performance is fundamentally coupled with energy management, and missions are often limited by the extent of onboard energy storage. Power beaming is an innovative method of decoupling an aircraft from onboard energy, thereby allowing unprecedented improvements in mission capabilities. However, it is challenging to design an aircraft that uses power beaming because remotely-powered aircraft are not subject to conventional energy-based scaling laws (which assume onboard energy storage) and because little to no empirical data exists for comparable designs. In this paper, we aim to discover the dominant variables that govern the design of power-beaming-enabled aircraft. We accomplish this by replacing traditional aircraft sizing methods with a novel, physics-based, large-scale design optimization framework.

The preliminary design process for traditional tube-and-wing aircraft often relies on statistical methods and energy-based formulas. Typical "black-box" statistical sizing and weight estimation methods have been presented and verified for conventional aircraft in preeminent aircraft design texts by Raymer [1], Roskam [2], and others. The Breguet range equation [3] is one example of a performance estimation method that assumes onboard liquid fuel. While these methods are powerful tools for designing conventional airplanes, they are not applicable to the unique configurations that are expected of an airplane that is optimized for power beaming. With this in mind, numerical optimization techniques are well poised to replace these conventional sizing methods when designing power-beaming-enabled aircraft. Primarily, this is because these techniques can be formulated in such a way that they rely upon specific physics-based models that are tailored to remotely-powered aircraft rather than on generalized formulas that are based on, for instance, well-understood conventional designs.

Recent advances in multidisciplinary design optimization (MDO) have proven that gradient-based optimization techniques are very successful at narrowing down the initial design-space for unique aircraft concepts in the presence of many (even hundreds) of variables. State-of-the-art examples include a study of the optimization of electric air taxis which is described by both Sarojini et al. [4] and Ruh et al. [5]. They introduce the Comprehensive Analysis and high-Dimensional DEsign Environment (CADDEE), and demonstrate the capabilities of CADDEE by solving an air-taxi design problem with more than 100 design variables in less than half an hour using a single processor on a desktop workstation. In another study targeting electric air mobility, Hwang and Ning utilized the widely used OpenMDAO framework [6] to maximize the range of NASA's X-57 Maxwell electric aircraft [7]. The optimized design demonstrated a range increase of 12%, and the optimization problem was solved in less than ten hours. Both of these examples of aircraft design optimization leverage an automatically implemented adjoint method to compute their derivatives [8]. The adjoint method scales well with increasing numbers of design variables, and is a key enabler of large-scale aircraft design optimization algorithms.

While power beaming is possible across the entire electromagnetic spectrum, laser sources near the optical wavelengths currently promise the highest transmission efficiencies due to the high degree of collimation that is possible with passive optics [9, 10]. The recent push for directed-energy systems with military applications has led to a series of successful field tests of lasers in the 100 kW range [11–13]. These lasers are considered to be sufficiently powerful, and their technical readiness to be high enough, that field demonstrations of large, unmanned, laser-powered aircraft are feasible in the near future [9, 14].

The current state of the art for laser-powered aircraft comprises feasibility studies [9, 15] and sub-scale flight demonstrations (e.g., quadcopters with potentially unlimited endurance [16], fixed-wing model airplanes [17], and insect-scale flapping robots [18]). Since no published designs exist for larger fixed-wing, laser-powered airplanes, there is not yet any consensus on which variables dominate the design of these airplanes. For example, the designer of a laser-powered airplane might wonder how close their airplane must fly to the ground-based laser source. Or the designer might want to add onboard batteries but wonders how much the extra weight will affect performance. This paper attempts to begin to answer these questions by proposing that large-scale design optimization is a tool that can rapidly compute optimal point-designs of laser-powered aircraft.

We begin this paper by describing our methodology. This includes the details of the sub-discipline models (power beaming, structures, thermal dissipation, propulsion, stability, and geometry parametrization) as well as the overall optimization problem formulation. Next, we present the results of a point-design optimization for an unmanned laser-powered airplane at high-altitude cruise. We use this airplane to perform four parameter sweeps, exploring the influence of additional payload weight, battery weight, altitude, and distance from the laser source on the airplane's total mass.

III. Methodology

As mentioned above, the large-scale design optimization framework which we propose relies upon physics-based models for power beaming, weight estimation, aerodynamics, thermal dissipation, and stability. These models are all written in the Computational System Design Language (CSDL) [19]. CSDL uses algorithms that act on computational graphs in order to automate adjoint-based sensitivity analysis for nearly any combination of mathematical operations. This significantly speeds up the process of model development and integration within an MDO framework.

In this paper we apply these models to the analysis and optimization of a twin-fuselage, high-altitude, unmanned airplane (Fig. 1). This electric aircraft is designed to carry a central power-beaming pod, that receives incoming laser power and converts it to electricity via an internal photoelectric array. This airplane has a conventional configuration that provides a basis for comparison with future work on unconventional configurations.

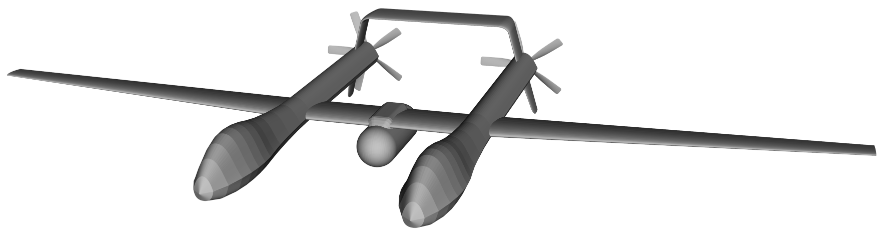

Fig. 1 The high-altitude, laser-powered airplane concept.

A. Analysis Models

1. Optical Power Beaming

The design of aircraft for laser power beaming relies heavily on models for high-energy beam propagation through the atmosphere. The High Energy Laser End-to-End Operational Simulation (HELEEOS) tool developed by the Air-Force Institute of Technology was explicitly designed to simulate high-power directed energy systems [20] and has been validated with a variety of experimental tests [21]. In this paper we use data from HELEEOS to construct an optical power-beaming model within our optimization problem framework. Specifically we train a Kriging [22] surrogate model using the SMT toolbox developed by Bouhlel et al. [23]. This model computes the power available at the aircraft as a function of the altitude, horizontal distance, velocity, and aperture size. The surrogate model (Fig. 2) is based on a 100 kW infrared laser (λ = 1 mm) with a one-meter diameter transmit aperture.

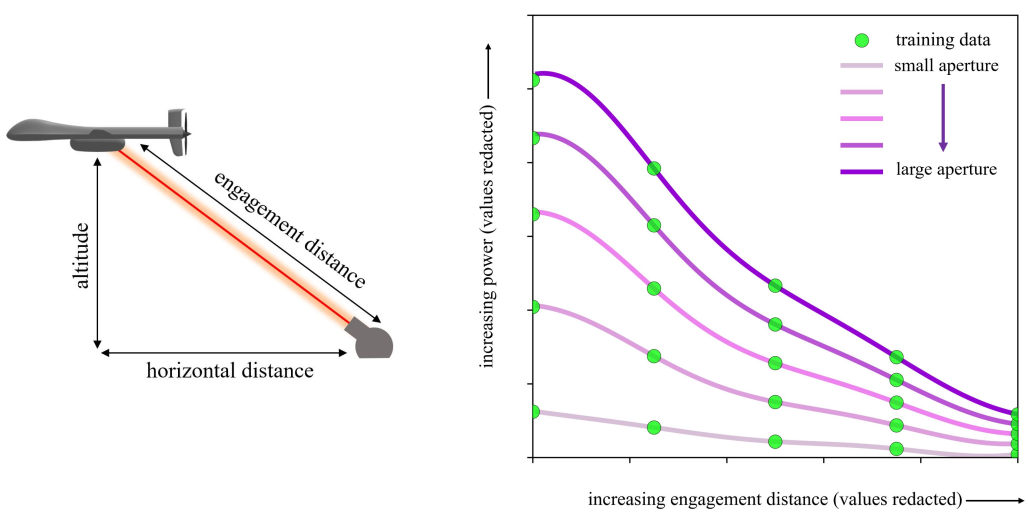

Fig. 2 Left: the laser engagement scenario. Right: the laser power-beaming model constructed using data from HELEEOS [20]. The figure shows available power as a function of receive aperture size and distance. The axes in this figure are redacted because they are based on confidential but unclassified information.

Using this power-beaming model, we construct a power-beaming residual as $R_{\text{o}} = P_{\text{available}} - P_{\text{required}}$. By constraining this residual ($R_{\text{o}} \geq 0$), we force the required power for cruise (P_{required}) to always be less than or equal to the available laser power ($P_{\text{available}}$).

2. Structural Weight Estimation

Many weight estimation techniques for preliminary aircraft design rely upon statistical methods or simple energy-based formulas. These methods allow the designer to estimate the weight of traditional concepts. However, aircraft designed to exploit power beaming tend towards unique configurations that defy traditional weight-estimation methods.

Laser-powered aircraft inherently require unique payloads to receive and potentially redirect laser power. These payloads have large optical apertures that drive the aircraft towards unique configurations. because these aircraft have little-to-no onboard power, the empty-weight fractions can be significantly lower than traditional aircraft.

Because of this, we implement a structural weight estimation model. This model extracts multiple one-dimensional meshes (Fig. 3) from the top-level aircraft geometry which represent various slender components such as the wing and the fuselage. We assign cross-sectional properties to each element in these meshes and then solve the resulting system for the elemental stresses. By modifying the structure to meet maximum allowable stress constraints, we can estimate the structural weight of any structural component.

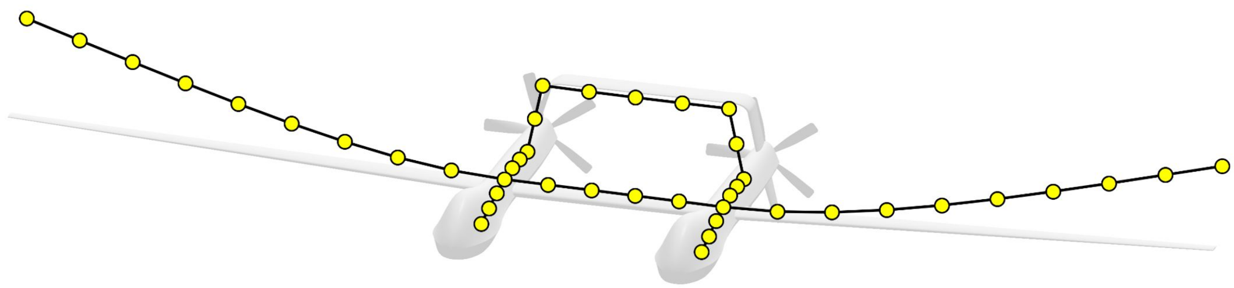

Fig. 3 The one-dimensional stick model representation of the aircraft structure (with exaggerated deflections).

To simplify the structural analysis, we approximate the wing-box structure as a hollow rectangular box-beam similar to the analysis performed by Chauhan and Martins [24] and by Sarojini [25]. The thicknesses of the box-beam web and cap (t_{web} and t_{cap}) are design variables in the optimization problem and the width and height of the beams are extracted from the wing meshes as ratios of the chord and the wing thickness. The two fuselage beams are modeled as thin-walled tubes of fixed diameter. Using these box-beam and tube elements, we construct a global stiffness matrix $[K]$ using 12×12 frame stiffness elements [26]. By combining the aerodynamic, inertial, and propulsive loads we create the stiffness matrix $\{F\}$ and then solve the linear system $\{F\} = [K]\{U\}$ for the displacements $\{U\}$.

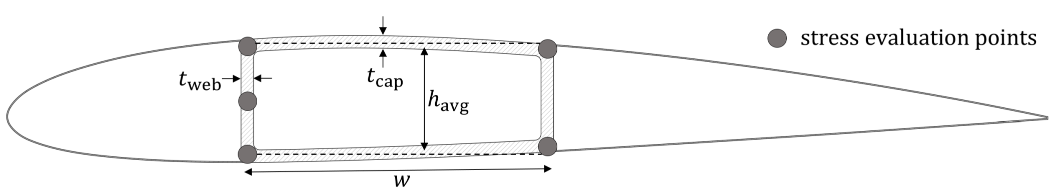

Fig. 4 The wing box structure is shown here with the stress evaluation points marked with circles.

After solving the linear system, we perform a stress recovery by using the local displacements to calculate the loads on each element in the global beam mesh. Using these loads we compute the stress at five points on the box beam (Fig. 4). These points correspond with the expected locations of the maximum bending stresses and the maximum shear stresses [24]. The aerodynamic and inertial loads in $\{F\}$ are multiplied by a load factor to capture a +3g sizing condition. Since no buckling models are included, we use a conservative two-times safety factor when evaluating the resulting Von-Mises stress at each of the five stress-evaluation points.

We validate the structural weight estimation model by optimizing the wing-box structure for NASA's hybrid-electric PEGASUS concept [27]. We compare the total wing mass from our 1D beam model with the optimized mass presented by Sarojini et al. [28], who presented results for an optimized wing structure using both 1D beam models and shell-based finite-element methods. Figure 5 shows this comparison. The beam model used here yields a total mass that is 8.2% greater than the referenced beam model and only 1.1% greater than the shell model. For the PEGASUS wing and the airplane in this paper we assume the material is aluminum 7050-T6 with a yield strength of 483 MPa and a density of 2700 kg/m^3.

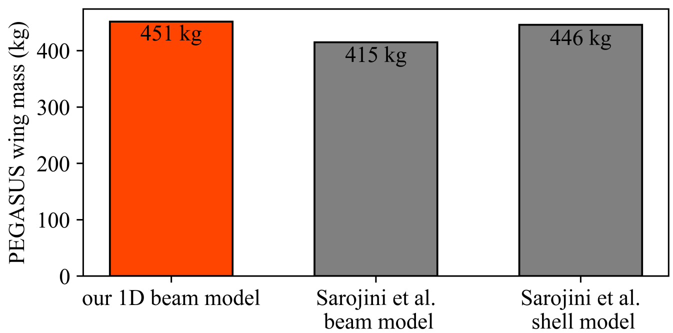

Fig. 5 The validation of our structural weight estimation model using data from Sarojini et al. [28] for the PEGASUS airplane wing [27].

3. Component Weight Estimation

The motors, rotors, battery, payload, and power-beaming systems must all be sized appropriately to guarantee that the aircraft's mass properties are accurate and the aircraft can be trimmed properly. For most of these systems we assume simple sizing relationships. For example, the motor mass is calculated as a function of the motor power (P_m), the motor power density b, and the motor efficiency η: $m = P_\mathrm{m}/(b\eta)$. The motor power is calculated to provide a rate-of-climb of 100 feet per minute by using the following relationship: $\dot{z} = (P_\mathrm{m} - P_\mathrm{req})/(mg)$ where the required power is the rotor power from the propulsion model. This guarantees that the aircraft is cruising at or below its service ceiling. The rotors are sized with a similarly simple relationship and the payload is treated as a point mass.

An aircraft that is powered remotely does not require an onboard battery. However, in the event of spontaneous cloud cover or other unforeseen events it can be a benefit to have some amount of onboard power. Because of this, we include half an hour of onboard battery power when computing the component weights. The battery energy density is assumed to be 200 W·h/kg.

Because the aperture size for the power-beaming pod affects the drag of the aircraft, we include a simple drag model that assumes a fixed drag coefficient ($C_D = 0.4$) normalized by the pod frontal area. With this model, we can capture the first-order effects that changes in aperture diameter (d_a) have on the aerodynamic forces on the aircraft. The pod mass is calculated using an assumed pod density of 75 kg/m^3 and a fixed pod length $L = 2$ m.

4. Thermal Dissipation

The proposed method of converting laser light to electricity relies on an internal photoelectric array. State-of-art photodiodes can achieve an efficiency greater than 60% for this optical-to-electrical conversion process[29]. Despite the promising conversion efficiency, the process of converting optical power to electrical power generates a significant thermal load on the aircraft. This thermal load depends on the aircraft design and the flight conditions, likely requiring 10-100 kW of heat dissipation to avoid overheating the airframe. The heat generated by the photoelectric array is transferred to the airplane structure before being dissipated into the atmosphere through a convection process.

Convection describes the heat transfer from an object caused by a flowing fluid. This process is complicated to model as it involves heat conduction and fluid motion, and the heat transfer rate varies significantly for different geometries and flow conditions. An accurate simulation for the heat convection process for an aircraft requires the use of either computational fluid dynamics (CFD) analysis [30] or experimental data [31]. The high-fidelity CFD analysis is too computationally expensive for the scope of the current study, and there is no experimental data available for laser-powered airplanes. Because of this, we make certain assumptions to provide a simple estimate for the heat transfer rate.

Our thermal dissipation model assumes an isothermal heat transfer analysis over the surface of the wing. The convection heat transfer rate is expressed as:

$$\dot{Q}_{\text{conv}} = hA(T_s - T_\infty), \tag{1}$$

where h is the convective heat transfer coefficient, T_s is the surface temperature, T_∞ is the temperature of the free-stream flow, and A is the surface area of the wing. The heat transfer rate is calculated from the Nusselt number which measures the ratio between the convection and conduction heat transfer rates. The Nusselt number is given by:

$$Nu = \frac{\dot{q}_{\text{conv}}}{\dot{q}_{\text{cond}}} = \frac{hL}{k}, \tag{2}$$

where k is the thermal conductivity of the air and L is the characteristic length. We use a forced heat correlation equation for smooth airfoils and compute the Nusselt number as [32]:

$$Nu = \left(0.0289\text{Re}^{0.81} - 257C_L^2\right)\text{Pr}^{1/3}, \tag{3}$$

where C_L is the lift coefficient of the wing, Re is the Reynolds number, and Pr is the Prandtl number defined as a function of the kinematic viscosity υ and the thermal diffusivity α:

$$\text{Pr} = \frac{\upsilon}{\alpha}. \tag{4}$$

5. Aerodynamics

The aerodynamic solver is used to compute the total aerodynamic forces and moments on the aircraft. We use mapped arrays to extract camber-surface meshes from the top-level aircraft geometry, which we then pass to a vortex-lattice method (VLM) solver. The VLM solver calculates the panel forces ($\boldsymbol{F}$) for all the lifting surfaces using the Kutta–Joukowski theorem [33]:

$$\boldsymbol{F} = \rho\boldsymbol{\Gamma}_{\text{b}}\boldsymbol{v}_{\text{ind}} \times \boldsymbol{s}. \tag{5}$$

In equation (5), the bound vortex circulation strength is Γ_b, the induced velocity at every vortex collocation point is $\boldsymbol{v}_{\text{ind}}$, $\boldsymbol{s}$ is the bound vector, and ρ is the atmospheric density (calculated from a standard atmosphere model). The panel forces are summed in the chord-wise direction and the moments are computed with respect to the quarter-chord point. The resulting 1-dimensional load vectors are connected to the 1-D beam model under the assumption that all the forces are conservative. This is a limiting assumption; however, we still recover the first-order effects that govern the changes in structural stress as the lifting surfaces are scaled during optimization. Any additional sources of drag (such as the fuselage and the vertical tail) are approximated with fixed drag-area estimates calculated using the parasite drag tools within OpenVSP [34].

6. Propulsion

Blade-element-momentum (BEM) rotor models combine momentum theory with airfoil theory to compute thrust and torque for a limited set of operating conditions. A modified form of the BEM tool developed by Ruh and Hwang [35] using CSDL is used in this study. The rotor power coefficient (C_P) is computed as a function of the torque coefficient (C_Q) as $C_P = 2\pi C_Q$, from which we calculate the rotor power, $P = \rho n^3 d^5 C_P$. The rotor power is then used to determine the corresponding motor mass and the total battery mass. The BEM model computes the total propulsive forces and moments for each rotor as a function of the aircraft states ($\vec{x}$) and the rotor speed. These loads are summed over all rotors to get the net propulsive forces and moments. These propulsive loads are then used to compute the trim residual described in the following section.

7. Equations of Motion

To guarantee a steady flight condition, we enforce a condition that all loads (aerodynamic, propulsive, and inertial) are balanced. We accomplish this by using the following equations of motion to compute a trim residual which is driven to zero as an equality constraint in the optimization problem (Table 1):

$$F_x - mg\sin\theta = m\left(\dot{u} + qw - rv\right) \tag{6}$$

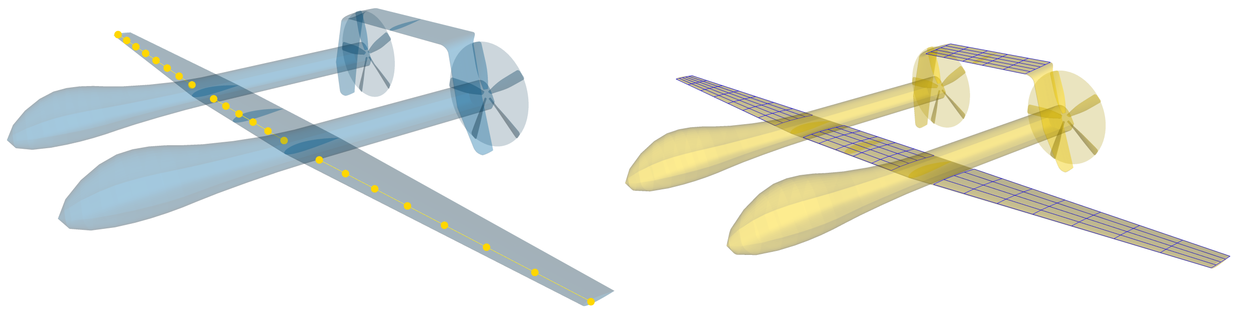

Fig. 6 Left: the 1-D beam meshes are placed along the quarter chord. Right: the aerodynamic mesh parametrization is shown here using mapped arrays to represent the camber-lines for all the lifting surfaces.

$$F_y + mg\cos\theta\sin\phi = m\left(\dot{v} + ru - pw\right) \tag{7}$$

$$F_z + mg\cos\theta\cos\phi = m\left(\dot{w} + pv - qu\right) \tag{8}$$

$$L = I_x\dot{p} - I_{yz}\left(q^2 - r^2\right) - I_{zx}\left(\dot{r} + pq\right) - I_{xy}\left(\dot{q} - rp\right) - \left(I_y - I_z\right)qr \tag{9}$$

$$M = I_y\dot{q} - I_{zx}\left(r^2 - p^2\right) - I_{xy}\left(\dot{p} + qr\right) - I_{yz}\left(\dot{r} - pq\right) - \left(I_z - I_x\right)rp \tag{10}$$

$$N = I_z\dot{r} - I_{xy}\left(p^2 - q^2\right) - I_{yz}\left(\dot{q} + rp\right) - I_{zx}\left(\dot{p} - qr\right) - \left(I_x - I_y\right)pq. \tag{11}$$

In equations (6-11) the total forces about the x, y, and z axes are F_x, F_y, and F_z respectively. The moments are L, M, and N. The linear velocity terms are u, v, and w, and the rotational velocities are p, q, and r. The Euler angles that rotate the body-fixed frame are ϕ, θ, and ψ. Given the aircraft states $\vec{x}$, the mass properties (m, $I_{(\cdot)}$), and the loads we calculate the accelerations $\dot{\vec{x}}$ in order to construct a trim residual ($\mathcal{R}$) [4]:

$$\mathcal{R} = \dot{\vec{x}}^T \cdot [W] \cdot \dot{\vec{x}}, \tag{12}$$

where $[W]$ is a positive-definite weighting matrix.

8. Geometry Parametrization and Representation

We initialize the optimization using a 3D model of the aircraft's outer mold line (OML) generated using OpenVSP [34]. Sub-discipline meshes (Fig. 6) are projected onto the geometry to create a parametric mapping from the OML. This representation of the geometry and meshes enables changes in the geometry to consistently propagate to changes in the solver inputs. The geometry is optimized using free-form deformations [36] (Fig. 7) with a custom-designed, low-dimensional parametrization to facilitate fast optimization with robust geometry manipulations. Other quantities such as the chord and twist distributions for the rotors are represented as B-spline curves where the control points of the curves are added as design variables in the optimization problem.

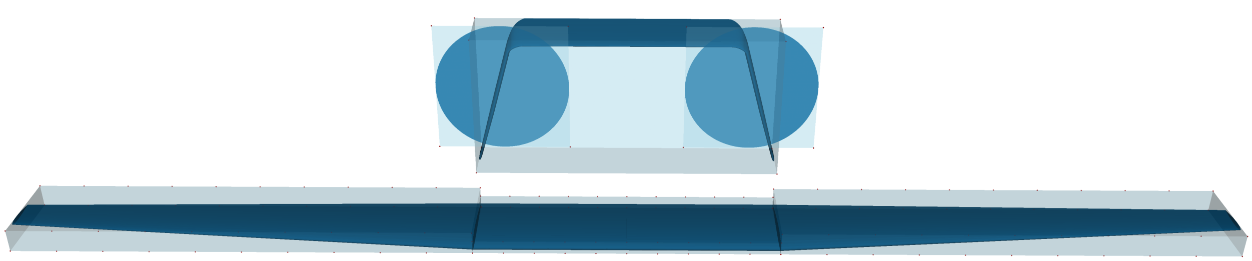

Fig. 7 The rotors and the lifting surfaces are enclosed within free-form deformation blocks, which scale the components during optimization.

B. Optimization Problem Formulation

Using the physics-based models presented previously, we formulate an optimization problem that allows us to optimize the electric unmanned airplane shown in figure 1. The objective of our optimization is to find the minimum total mass for a specified high-altitude cruise condition. We choose to minimize mass because mass is strongly correlated with a variety of important factors in aircraft design (e.g., performance and cost). The complete optimization problem is summarized in Table 1, and the design structure matrix can be seen in figure 8.

Table 1 Optimization problem formulation

Objective	Mass	m	Quantity
Design variables	Wing span	b	1
	Center span	b_c	1
	Tail incidence	i_{ht}	1
	Pitch angle	θ	1
	Mach number	m	1
	Payload cg	cg_x	1
	Left/right rotor speed	n	2
	Aperture diameter	d_a	1
	Rotor diameter	d_r	1
	Wing beam cap thickness	t_{cap}	20
	Wing beam web thickness	t_{web}	20
			Total design variables: 50
Constraints	Static margin	$\text{SM} \geq 0$	1
	Maximum mach number	$m \leq 0.3$	1
	Endurance	$e = 0.5$ hrs	1
	Optical power residual	$R_o \geq 0$	1
	Trim residual	$\mathcal{R}(\dot{\vec{x}}) = 0$	1
	Maximum stress	$\max(\sigma) \leq \sigma_{\max}$	1
	Minimum beam thickness	$\min(t) \geq 1e^{-3}$ m	1
	Maximum rotor diameter	$\max(d) \leq 3$ m	1
	Maximum surface temperature	$T_s \leq T_{\max}$	1
	Maximum center-span distance	$\lvert b_c \rvert \leq 2$ m	1
			Total constraints: 9

The cruise altitude is fixed at 18,288 m (60,000 ft), the horizontal distance from the laser source is 350 km, and the payload weight is 50 kg. These are the only fixed parameters governing the cruise condition. Other parameters such as Mach number and pitch angle are design variables. The atmospheric properties (density, pressure, and temperature) at this altitude are taken from a standard-atmosphere surrogate model, constructed using a sixth-order polynomial regression.

The geometric design variables are the wing span, the center-wing span, and the horizontal-tail incidence. These variables are the minimum necessary that allow the optimizer to find a feasible solution (primarily by varying the wing area to generate more or less lift). The horizontal-tail incidence is a critical variable when computing the trim residual ($\mathcal{R}$) because the tail cancels out the aerodynamic moment from the wing. The wing incidence angle is not a design variable. Instead, the pitch angle for the entire airplane is a design variable, which effectively changes the incidence of the wing.

Perhaps the most important constraint is the maximum allowable stress. Because the objective of the optimization problem is the total mass, the structural solution will inherently be driven to the maximum stress constraint. Another important constraint is the maximum Mach number, which is limited to 0.3, above which the incompressible-flow assumptions within the VLM solver begin to break down. Because of the limited power available, we find that the optimizer drives the design to a negative static margin. This increases aerodynamic efficiency (by requiring less negative tail incidence) but results in an airplane that is not passively longitudinally stable. Because of this, we also include a constraint that the static margin must be greater than zero. This effectively constrains the locations at which the heavier components (the battery and payload) can be placed. To limit the total number of constraints, we use maximum and minimum operators on all the vectorized constraints (e.g., maximum stress). Since the maximum and minimum operations are non-differentiable we approximate these constraints using Kreisselmeier-Steinhauser functions.

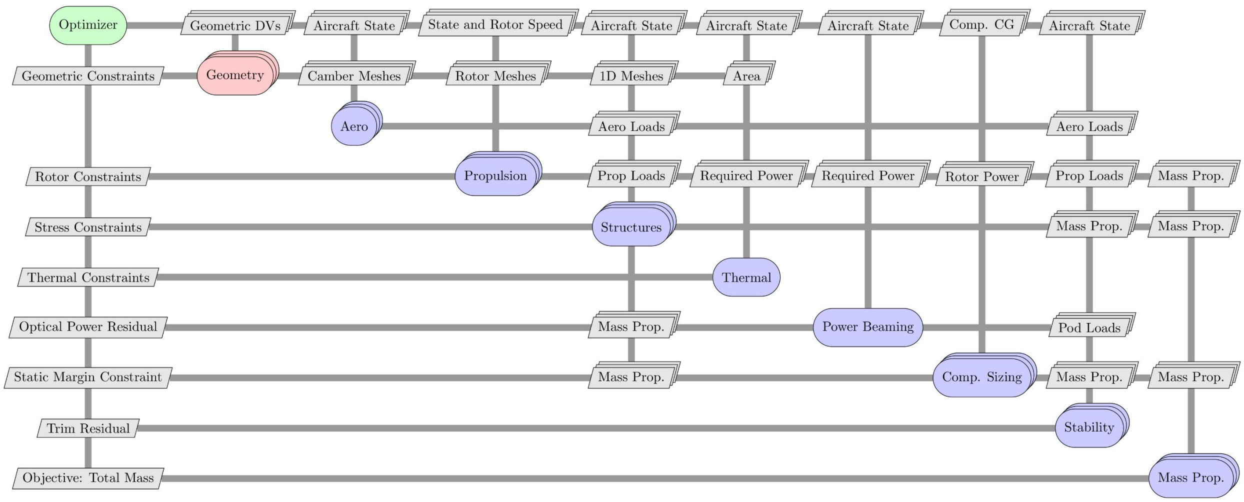

Fig. 8 The design structure matrix for the optimization problem. The diagonal, blue elements are the sub-discipline solvers and the red geometry element extracts the solver meshes from the top-level aircraft geometry.

The optimizer is SNOPT-7.7 [37] (a sparse nonlinear optimizer), which in most cases converges to an optimal solution within 25 minutes using a desktop computer with an Intel i7-13700K processor and 32 GB of memory.

IV. Results

Using the models and the optimization problem formulation outlined previously, we conduct an optimization study for the aircraft shown in figure 1 flying at 60,000 ft. Because the large-scale optimization approach presented here is intended to replace the preliminary design process, minimal effort was given to the design of the original airplane concept. In fact, a major result of this paper is that the optimizer was able to take the original design and find a feasible solution as well as an optimal one.

A. High-altitude cruise optimization

The optimal airplane design is shown in figure 9 as well as the original design. The original design is sub-optimal *and* infeasible while the final design is both feasible (i.e., satisfies the constraints) and optimal. This is an important note, since it demonstrates that the MDO problem can perform the bulk of the initial airplane sizing on its own, with very little analytical work by the designer.

The optimized design (Fig. 9) has a wingspan of 18.9 m (62 ft), a total mass of 262 kg, and flies at Mach 0.18. This mass at first seems very low for an aircraft of this size. However, we remind the reader that the airplane carries very little onboard energy (0.5 hr battery endurance) which results in a lighter-than-expected airplane. The rotors require a combined 7.5 kW of power, which results in a total powertrain systems mass of 56 kg (motor and rotor masses). Because the power required is relatively low compared to the source laser (100 kW), the required aperture diameter is only 0.29 m, and since the pod mass is a function of the aperture size, this aperture size is the minimum that enables the aircraft to maintain steady flight (with optical power residual $R_o \approx 0$).

The deflection of the outer wing segments for the optimized airplane is shown in figure 10. The deflection at the wing tip is nearly 1.75 m. This certainly violates the conservative force assumption that we made earlier. However, the stress distribution and cap thicknesses match our intuition. Figure 10 shows that the Von-Mises stress is at the stress limit across the majority of the span, before falling to zero at the tip (due to the minimum thickness constraint for the wing-beam web and cap). This is exactly the expected behavior for a minimum-mass cantilever beam.

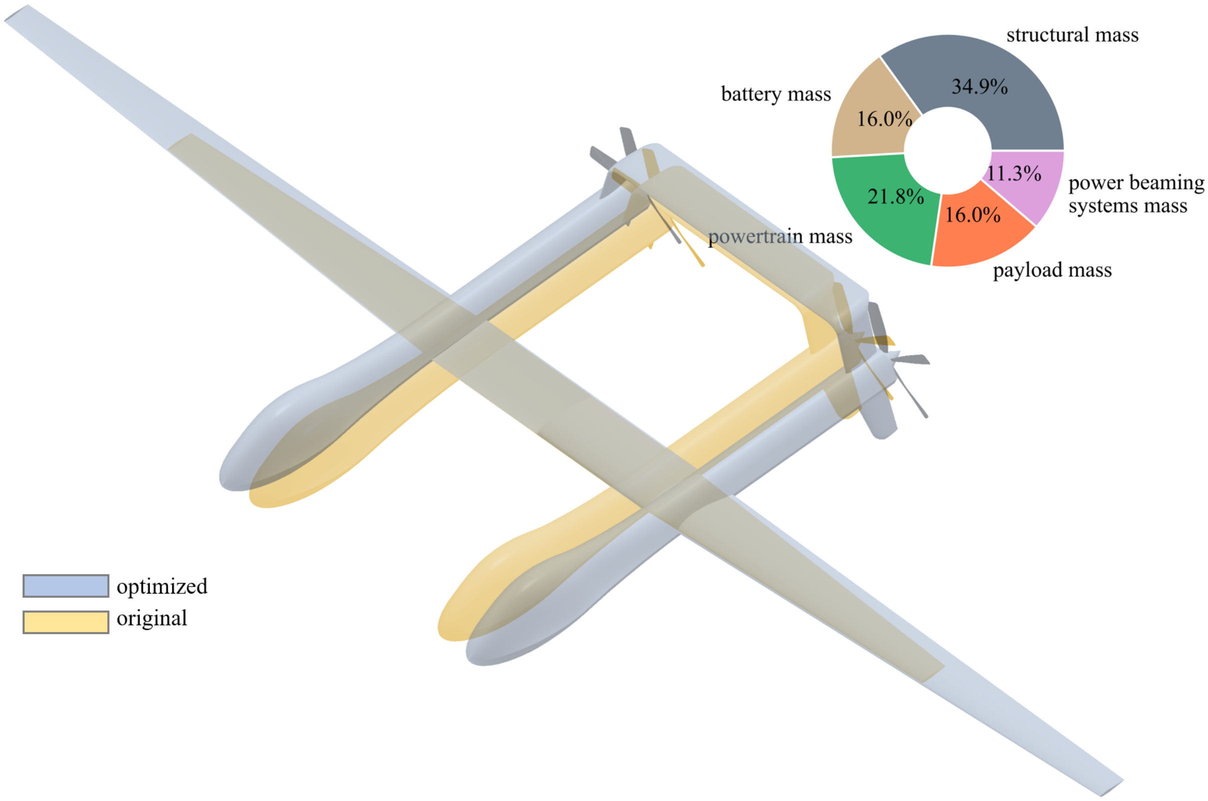

Fig. 9 The original (yellow) and optimal (blue) laser-powered airplane designs. The mass properties are shown at the top right of the figure.

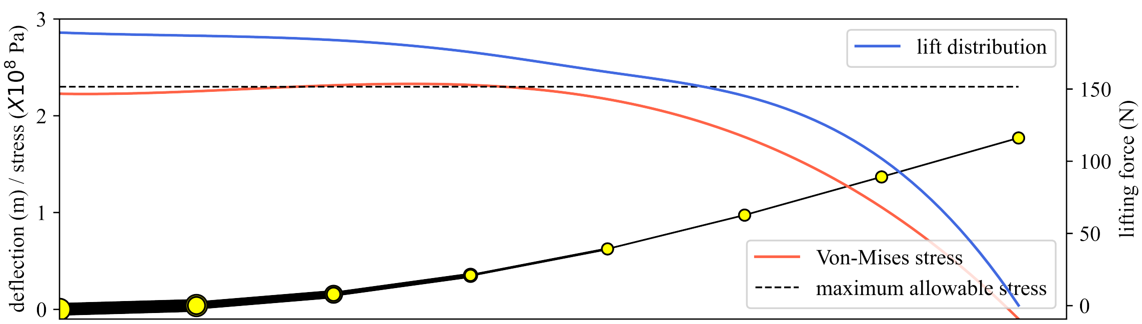

Fig. 10 The results of the structural optimization are shown here for the entire outer wing segments. The line thickness represents the box-beam cap thickness (not proportional), which is a design variable in the optimization problem.

B. Parameter sweeps

By varying certain fixed parameters from the previous results, we investigate the effect of several parameters on the total mass of the airplane.

Figure 11 shows the results of parameter sweeps for payload mass and required battery endurance. These sweeps were conducted at a constant altitude (60,000 ft) and the battery endurance was fixed at 0.5 hours when varying the payload mass and the payload mass was fixed at 50 kg when varying battery endurance. Figure 12 shows sweeps of operating altitude and horizontal distance from the laser source. The sweep of operating altitude were conducted with a fixed 50 kg payload and 0.5 hour battery endurance and the sweep of horizontal distance was performed at an altitude of 60,000 ft and the same payload and battery endurance.

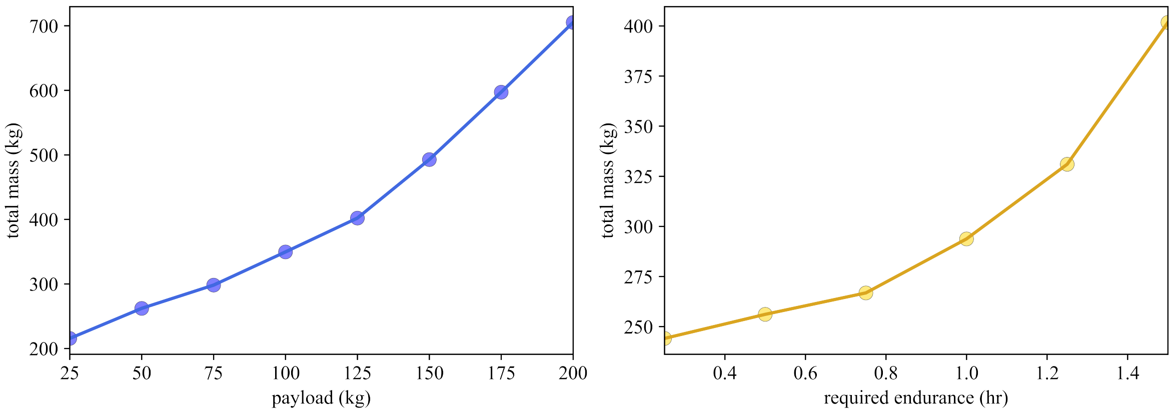

Fig. 11 Left: total mass versus payload. Right: total mass versus battery endurance (with a fixed 50 kg payload).

In figure 11 we see a nearly-linear relationship between payload mass and total mass. However, the linear relationship is quite steep (from 225 kg to 706 kg or roughly 2.75 kg total mass per kg of payload). This is primarily because of the increased structural mass required to carry the heavier payloads. Figure 11 also shows a clear exponential increase in total mass with regards to the required battery endurance (240 kg with half an hour of endurance and 410 kg with 1.5 hours endurance). This is because the increased endurance requires a larger battery, which requires more structural mass, which in turn requires more rotor power. For both these parameter sweeps the optimization problem would not converge past 200 kg payloads and 1.5 hr battery endurance. This does not mean that the problem is infeasible past these points. It simply indicates that the problem scaling and the initial design point are too far from optimal/feasible to result in a converged solution (due to numerical difficulties and poorly conditioned matrices).

There is a clear minimum near 30,000 ft in the plot of total mass versus altitude (Fig. 12). This is unexpected since the higher atmospheric density at low altitudes should yield a smaller wing, which should decrease the total mass. However, certain geometric constraints become active at low altitudes (rotor diameter, and center-span distance) that are likely restricting the design space.

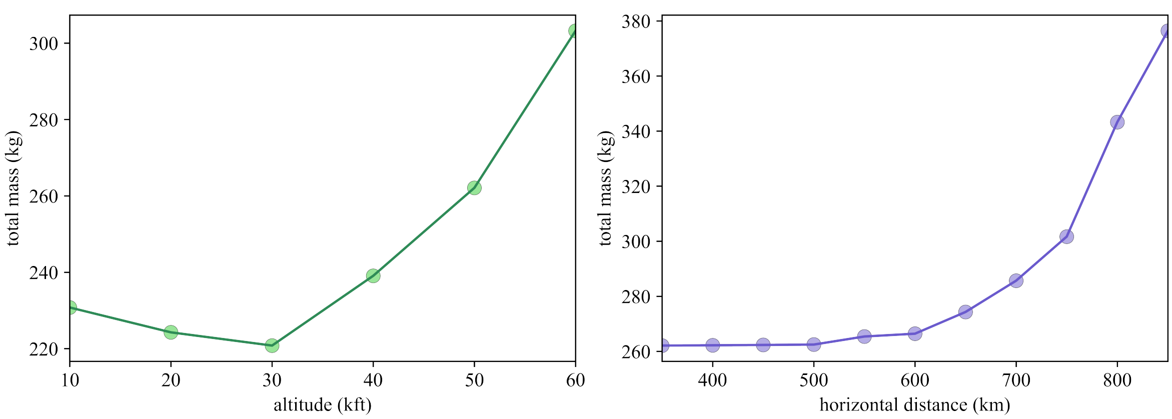

Fig. 12 Left: total mass versus operating altitude. Right: total mass versus horizontal distance from the ground-based laser source (assuming a fixed altitude of 50,000 ft).

With increasing horizontal distance from the ground-based laser source (Fig. 12), the total mass increases very slowly through 600 km and then increases rapidly through 850 km. This mass increase has a strong correlation with required aperture size, which begins near 0.2 m and ends near 0.8 m. Consequently, the mass of the pod increases, leading to an overall increase in total mass. What is particularly noticeable about this result is that the total mass is relatively flat through 600 km, perhaps suggesting that laser-powered airplanes such as the one in this paper must stay within a certain range of the laser source before their size becomes impractical.

V. Conclusion

In this paper we explore the sensitivity of the sizing of a laser-powered unmanned aircraft to various design parameters. We do this by formulating a large-scale multidisciplinary design optimization problem using physics-based models for laser power beaming, aerodynamics, structures, and stability. Using this optimization problem we demonstrate the ability to find aircraft designs that are both feasible and optimal, something that is not necessarily guaranteed for such a novel application.

We perform four parameter sweeps. First we vary the payload mass from 25 kg to 200 kg, and find that the total airplane mass increases nearly linearly from 225 kg to 706 kg. Second, we vary the amount of onboard battery power by varying the battery-only endurance from half an hour to 1.5 hours. We find that the total mass increases exponentially with required endurance, indicating that the airplane is very sensitive to this requirement. Third, we vary the operating altitude from 10,000 ft to 60,000 ft. This parameter sweep clearly demonstrates a minimum mass at an altitude of 30,000 ft. However, below this point several constraints become active that limit the design space. Finally, we explore the affect of horizontal distance from the ground-based laser source. This plot shows that the total mass remains roughly flat through 600 km, before increasing rapidly. This suggests that laser-powered airplanes such as the one in this paper must fly within a limited range from their power source before their mass becomes impractical.

Overall, our work demonstrates that large-scale multidisciplinary design optimization can replace existing preliminary design methods (e.g., empirical data and energy-based formulas) for power-beaming-enabled aircraft. The method that we propose is robust and could be applied to a wide variety of aircraft configurations in power-beaming scenarios, which would allow us to find the true minimums in the design space. Future work will explore different aircraft configurations and investigate additional parameters, with a focus on both verification and validation of our results.

Acknowledgments

The material presented in this paper is, in part, based upon work supported by DARPA under grant No. D23AP00028-00 and by NASA under award No. 80NSSC21M0070.

References

[1] Raymer, D., *Aircraft design: a conceptual approach*, American Institute of Aeronautics and Astronautics, Inc., 2012.

[2] Roskam, J., *Airplane design*, DARcorporation, 1989.

[3] Anderson, J. D., and Bowden, M. L., *Introduction to flight*, Vol. 582, McGraw-Hill Higher Education New York, 2005.

[4] Sarojini, D., Ruh, M. L., Joshy, A. J., Yan, J., Ivanov, A. K., Scotzniovsky, L., Fletcher, A. H., Orndorff, N. C., Sperry, M., Gandarillas, V. E., et al., "Large-Scale Multidisciplinary Design Optimization of an eVTOL Aircraft using Comprehensive Analysis," *AIAA SCITECH 2023 Forum*, 2023. https://doi.org/10.2514/6.2023-0146.

[5] Ruh, M., Joshy, A. J., Fletcher, A., Asher, I., and Hwang, J., "Large-scale multidisciplinary design optimization of the NASA lift-plus-cruise concept using a novel aircraft design framework," *VFS*, 2023. https://doi.org/10.48550/arXiv.2304.14889.

[6] Gray, J. S., Hwang, J. T., Martins, J. R. R. A., Moore, K. T., and Naylor, B. A., "OpenMDAO: An open-source framework for multidisciplinary design, analysis, and optimization," *Structural and Multidisciplinary Optimization*, Vol. 59, No. 4, 2019, pp. 1075–1104. https://doi.org/10.1007/s00158-019-02211-z.

[7] Hwang, J. T., and Ning, A., "Large-scale multidisciplinary optimization of an electric aircraft for on-demand mobility," *2018 AIAA/ASCE/AHS/ASC Structures, Structural Dynamics, and Materials Conference*, 2018, p. 1384. https://doi.org/10.2514/6.2018-1384.

[8] Hwang, J. T., and Martins, J. R., "A computational architecture for coupling heterogeneous numerical models and computing coupled derivatives," *ACM Transactions on Mathematical Software (TOMS)*, Vol. 44, No. 4, 2018, pp. 1–39. https://doi.org/10.1145/3182393.

[9] Mason, R., "Feasibility of laser power transmission to a high-altitude unmanned aerial vehicle," Tech. rep., Rand Project Air Force Santa Monica CA, 2011.

[10] Huo, Y., Dong, X., Lu, T., Xu, W., and Yuen, M., "Distributed and Multilayer UAV Networks for Next-Generation Wireless Communication and Power Transfer: A Feasibility Study," *IEEE Internet of Things Journal*, Vol. 6, No. 4, 2019, pp. 7103–7115. https://doi.org/10.1109/JIOT.2019.2914414.

[11] Lamberson, S., Schall, H., and Shattuck, P., "The airborne laser," *XVI International Symposium on Gas Flow, Chemical Lasers, and High-Power Lasers*, Vol. 6346, SPIE, 2007, pp. 471–478. https://doi.org/10.1117/12.738802.

[12] Forden, G., "The airborne laser," *IEEE Spectrum*, Vol. 34, No. 9, 1997, pp. 40–49. https://doi.org/10.1109/6.619379.

[13] Shwartz, J., Wilson, G. T., and Avidor, J. M., "Tactical high-energy laser," *Laser and Beam Control Technologies*, Vol. 4632, SPIE, 2002, pp. 10–20. https://doi.org/10.1117/12.469758.

[14] Bar-Cohen, A., Felbinger, J., and Sivananthan, A., "Department of Defense Power Beaming Roundtable," 2015.

[15] Nugent Jr, T. J., and Kare, J. T., "Laser power beaming for defense and security applications," *Unmanned systems technology XIII*, Vol. 8045, 2011, pp. 384–391. https://doi.org/10.1117/12.886169.

[16] Achtelik, M. C., Stumpf, J., Gurdan, D., and Doth, K.-M., "Design of a flexible high performance quadcopter platform breaking the MAV endurance record with laser power beaming," *2011 IEEE/RSJ International Conference on Intelligent Robots and Systems*, 2011, pp. 5166–5172. https://doi.org/10.1109/IROS.2011.6094731.

[17] Blackwell, T., "Recent demonstrations of Laser power beaming at DFRC and MSFC," *AIP Conference Proceedings*, Vol. 766, No. 1, 2005, pp. 73–85. https://doi.org/10.1063/1.1925133.

[18] James, J., Iyer, V., Chukewad, Y., Gollakota, S., and Fuller, S. B., "Liftoff of a 190 mg Laser-Powered Aerial Vehicle: The Lightest Wireless Robot to Fly," *2018 IEEE International Conference on Robotics and Automation (ICRA)*, 2018, pp. 3587–3594. https://doi.org/10.1109/ICRA.2018.8460582.

[19] Gandarillas, V., Joshy, A. J., Sperry, M. Z., Alexander Ivanov, and Hwang, J. T., "A graph-based methodology for constructing computational models that automates adjoint-based sensitivity analysis," *Structural and Multidisciplinary Optimization*, 2023.

[20] Fiorino, S., Bartell, R., Perram, G., Bunch, D., Gravley, L., Rice, C., Manning, Z., Krizo, M., Roadcap, J., and Jumper, G., "The HELEEOS Atmospheric Effects Package: A Probabilistic Method for Evaluating Uncertainty in Low-Altitude, High-Energy Laser Effectiveness," *Journal of Directed Energy [JDE] JDE*, Vol. 26, No. 17, 2006, p. 47.

[21] Fiorino, S. T., Randall, R. M., Bartell, R. J., Haiducek, J. D., Spencer, M. F., and Cusumano, S. J., "Field measurements and comparisons to simulations of high energy laser propagation and off-axis scatter," *Free-Space Laser Communications X*, Vol. 7814, SPIE, 2010, pp. 186–196. https://doi.org/10.1117/12.860046.

[22] Sacks, J., Schiller, S. B., and Welch, W. J., "Designs for computer experiments," *Technometrics*, Vol. 31, No. 1, 1989, pp. 41–47. https://doi.org/10.2307/1270363.

[23] Bouhlel, M. A., Hwang, J. T., Bartoli, N., Lafage, R., Morlier, J., and Martins, J. R. R. A., "A Python surrogate modeling framework with derivatives," *Advances in Engineering Software*, 2019, p. 102662. https://doi.org/https://doi.org/10.1016/j.advengsoft.2019.03.005.

[24] Chauhan, S. S., and Martins, J. R., "Low-fidelity aerostructural optimization of aircraft wings with a simplified wingbox model using OpenAeroStruct," *EngOpt 2018 Proceedings of the 6th International Conference on Engineering Optimization*, Springer, 2019, pp. 418–431. https://doi.org/10.1007/978-3-319-97773-7_38.

[25] Sarojini, D., "Structural analysis and optimization of aircraft wings through dimensional reduction," Ph.D. thesis, Georgia Institute of Technology, 2021.

[26] Logan, D. L., *First Course in the Finite Element Method, Enhanced Edition, SI Version*, Cengage Learning, 2022.

[27] Antcliff, K. R., and Capristan, F. M., "Conceptual design of the parallel electric-gas architecture with synergistic utilization scheme (PEGASUS) concept," *18th AIAA/ISSMO multidisciplinary analysis and optimization conference*, 2017, p. 4001. https://doi.org/10.2514/6.2017-4001.

[28] Sarojini, D., Solano, D., and Mavris, D. N., "Structural Layout Design Space Exploration and Structural Sizing of Aircraft Wingbox," *AIAA SCITECH 2022 Forum*, 2022, p. 1026. https://doi.org/10.2514/6.2022-1026.

[29] Kimukin, I., Biyikli, N., Butun, B., Aytur, O., Unlu, S. M., and Ozbay, E., "InGaAs-based high-performance pin photodiodes," *IEEE Photonics Technology Letters*, Vol. 14, No. 3, 2002, pp. 366–368. https://doi.org/10.1109/68.986815.

[30] Pellissier, M., Habashi, W., and Pueyo, A., "Optimization via FENSAP-ICE of aircraft hot-air anti-icing systems," *Journal of Aircraft*, Vol. 48, No. 1, 2011, pp. 265–276. https://doi.org/10.2514/1.C031095.

[31] Strobl, T., Storm, S., Thompson, D., Hornung, M., and Thielecke, F., "Feasibility study of a hybrid ice protection system," *Journal of Aircraft*, Vol. 52, No. 6, 2015, pp. 2064–2076. https://doi.org/10.2514/1.C033161.

[32] Samadani, S., and Morency, F., "Heat transfer correlations for smooth and rough airfoils," *Fluids*, Vol. 8, No. 2, 2023, p. 66. https://doi.org/10.3390/fluids8020066.

[33] Katz, J., and Plotkin, A., *Low-speed aerodynamics*, Vol. 13, Cambridge university press, 2001.

[34] McDonald, R. A., and Gloudemans, J. R., "Open vehicle sketch pad: An open source parametric geometry and analysis tool for conceptual aircraft design," *AIAA SciTech 2022 Forum*, 2022, p. 0004. https://doi.org/10.2514/6.2022-0004.

[35] Ruh, M. L., and Hwang, J. T., "Robust Modeling and Optimal Design of Rotors Using Blade Element Momentum Theory," *AIAA Aviation Forum*, 2021. https://doi.org/10.2514/6.2021-2598.

[36] Samareh, J. A., "A survey of shape parameterization techniques," *CEAS/AIAA/ICASE/NASA Langley International Forum on Aeroelasticity and Structural Dynamics 1999*, 1999.

[37] Gill, P. E., Murray, W., and Saunders, M. A., "SNOPT: An SQP algorithm for large-scale constrained optimization," *SIAM review*, Vol. 47, No. 1, 2005, pp. 99–131. https://doi.org/10.1137/S0036144504446096.